

RESEARCH PAPER

## Solvothermal -Assisted Cushy Precipitation Method of Like-Cauliflower Zinc Ferrite ( $ZnFe_2O_4$ ) Nanoparticles Using Hexamethylenetetramine (Hexamine) As a Non-ionic Surfactant

Ali Ameer Abd Zaid <sup>1</sup>, Luma M. Ahmed <sup>1\*</sup>, Rajaa K. Mohammad <sup>2</sup>

<sup>1</sup> Department of Chemistry, College of Science, University of Kerbala, Kerbala, Iraq

<sup>2</sup> Department of Physics, College of Science, University of Kerbala, Kerbala, Iraq

### ARTICLE INFO

#### Article History:

Received 06 October 2022

Accepted 24 December 2022

Published 01 January 2023

#### Keywords:

Alkali blue 4B dye

Non- ionic surfactant

Normal Spinel

Solvothermal method

Zinc ferrite nanoparticle

### ABSTRACT

Normal Spinel Zinc ferrite ( $ZnFe_2O_4$  or  $ZnO.Fe_2O_3$ ) nanoparticle has been synthesized as a dark reddish brown powder using precipitation method. The solvothermal method assisted the preparation route using ethanol at 180 °C for 90 min. The non-ionic surfactant Hexamethylenetetramine (hexamine) is employed as a capping agent, stabilizer and template. The XRD datum demonstrated the  $ZnFe_2O_4$  peaks were embedded in an amorphous matrix giving broad peaks with a small mean crystal size (16.98 nm). The SEM analysis revealed the  $ZnFe_2O_4$  was found to be homogenous agglomerated like-cauliflower, with particle size 27.78 nm. The EDX analysis evidence the  $ZnFe_2O_4$  was purely prepared from Zn, Fe and O in wt % equal 100. The FT-IR analysis proved the  $ZnFe_2O_4$  nanoparticle is synthesis as a normal spinel type, and found two reasonable peaks of M-O bond in crystal lattices of  $ZnFe_2O_4$  nanoparticle first for ( $Fe^{3+} - O^{2-}$ ) octahedral site and the other for ( $Zn^{2+} - O^{2-}$ ) tetrahedral sits for. The band gap found to be 2.10 eV as an indirect band gap. The best dose of spinel to decolorize alkali blue 4B dye was 0.025 g/ 100 mL with efficiency 97.3 % at 30 min. The high increased in  $ZnFe_2O_4$  dose leads to the screen effect. The photodecolorization of dye obeys to pseudo-first order, and the activation energy is found to be 47.689 kJ/mol at temperature raged (15-35) °C. This photoreaction is endothermic and non-spontaneous that attributed to the raise in the solvation of the transition state between dye and hydroxyl radical.

### How to cite this article

Zaid A A., Ahmed L M., Mohammad R K. Solvothermal -Assisted Cushy Precipitation Method of Like-Cauliflower Zinc Ferrite ( $ZnFe_2O_4$ ) Nanoparticles Using Hexamethylenetetramine (Hexamine) As a Non-ionic Surfactant. J Nanostruct, 2023; 13(1):193-203. DOI: 10.22052/JNS.2023.01.021

### INTRODUCTION

Nanotechnology is a fascinating field that works with particles that are smaller than 100 nanometers. The high surface-to-volume ratio of these particles is due to their small size. To put it another way, these particles contain a lot of active

sites, which boosts their activity dramatically. In the literature, a variety of nanomaterials for various uses have been reported[1]. As magnetic materials, spinel ferrites are often used. Numerous metal oxides, mixed metal oxides, and ferrites have shown heightened sensitivity to certain

\* Corresponding Author Email: [luma.ahmed@uokerbala.edu.iq](mailto:luma.ahmed@uokerbala.edu.iq)



This work is licensed under the Creative Commons Attribution 4.0 International License.

To view a copy of this license, visit <http://creativecommons.org/licenses/by/4.0/>.

gases and humidity. The spinel's form is in a face-centered cubic (FCC) lattice with eight formula units per cubic unit cell, which corresponds to the space group  $Fd_3m$  ( $O_7^h$ ).  $(M^{2+})_t [Fe_2^{3+}]_o O_4^{2-}$  is the usual molecular formula of spinel ferrites, where  $M^{2+}$  and  $Fe^{3+}$  are the divalent and trivalent cations occupying tetrahedral (A) and octahedral (B) interstitial spaces of the FCC lattice formed by  $O^{2-}$  ions. Spinel structures include both normal spinel and inverse spinel structures. As magnetic materials, spinel ferrites are often used. Numerous metal oxides, mixed metal oxides, and ferrites have shown heightened sensitivity to certain gases and humidity. The unfilled octahedral, tetrahedral, and tetrahedral holes may accommodate the analyzed species and may function as an efficient sensor. Cobalt ferrite ( $CoFe_2O_4$ ), Copper ferrite ( $CuFe_2O_4$ ), and Nickel ferrite ( $NiFe_2O_4$ ) are inverse spinel's with ferric ions occupying tetrahedral (A) sites and ferric ions and the specific metal ions occupying octahedral (B) sites, as in  $[(Fe^{3+})^A] [M^{2+} Fe_2^{3+}]^B O_4^{2-}$ .  $ZnFe_2O_4$  has a conventional spinel structure, with  $Zn^{2+}$  and  $Fe^{3+}$  occupying tetrahedral and octahedral sites, respectively [2]. Zinc ferrite is a normal spinel oxide with a cubic structure and considerable potential for use in gas sensors and other technological applications [3], magnetic and superparamagnetic materials[4], adsorbents[5], materials with optical and dielectric properties[6], antibacterial agent[7], catalysts and photocatalysts [8]. As a typical n-type semiconductor photocatalyst, spinel zinc ferrite ( $ZnFe_2O_4$ , ZFO) has a very narrow bandgap (1.9 eV), allowing ZFO to capture around 46% of the sun's energy for the creation of photogenerated electrons ( $e^-$ ) and holes ( $h^+$ ). In the preceding decade, ZFOs were extensively employed as reusable magnetic photocatalysts for the removal of dyes, organic contaminants, microcystin-LR, and bacteria. Although ZFO has a broad light absorption range, its catalytic activity is poor due to the rapid recombination of photogenerated  $e^-$  and  $h^+$ . As reported by Deng and et al[9], ion doping will alter the coordination relationship between the iron (Fe) atom and oxygen atom in the ZFO lattice. Specifically, some formerly octahedral coordinated Fe atoms (FeO) are converted to tetrahedral coordinated Fe atoms (Fe T), and the transport of the  $e^-$  can be facilitated by the super exchange interaction. Dyeing businesses such as textiles and tanneries produce effluents containing dye that are hazardous and need treatment. In the

last years, it has seen an increase in the use of advanced oxidation processes (AOPs) to remove organic contaminants from aqueous solutions. Among the AOPs, the heterogeneous Fenton reaction is one of the most interesting processes since it employs solid iron-based catalysts and their simple recovery after treatment by a magnetic field allows for their reuse. However, little research has been published on the utilization of zinc ferrite for the breakdown of organic contaminants via the heterogeneous Fenton process under visible light irradiation [10]. The synthesis of zinc ferrite oxide with the necessary physical properties for usage in a range of research fields has been a major focus. So,  $ZnFe_2O_4$  ternary oxide has been produced in several methods, including precipitation followed by calcination, succinic acid-assisted hydrothermal route, electrospinning, surfactant-assisted hydrothermal synthesis, sol-gel technique followed by calcination, glycine combustion, solvothermal synthesis, sol-gel auto combustion reaction, polyethylene glycol-assisted route, and hydrothermal method in the presence of polyethylene glycol[11]. This work aims to prepare normal spinel  $ZnFe_2O_4$  using the precipitation method in presence of non-ionic surfactant (hexamine). This synthesis method is assisted by the solvothermal method using ethanol at 180 °C at 90 min. The characterization of prepared  $ZnFe_2O_4$  will measure using XRD, SEM-EDX, FT-IR and Bg. The normal spinel  $ZnFe_2O_4$  will apply in the decolonization of dye.

## MATERIALS AND METHODS

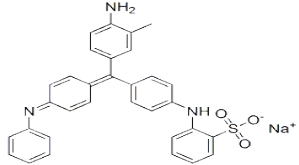
### Materials

The powder of Ferric nitrate  $Fe(NO_3)_3 \cdot 9H_2O$  and Zinc nitrate  $Zn(NO_3)_2 \cdot 9H_2O$  were supplied by sigma cheml co. Ammonia solution (25 %), absolute ethanol ( $C_2H_5OH$ ) and hexamethylenetetramine (hexamine) were purchased by Merck, BDH and Interchimiques SA, respectively. The alkali blue 4B dye was supplied from Merck and had information as flowing in Table 1.

### Synthesis of Spinel $ZnFe_2O_4$ nanocrystals

This procedure was modified from reference [12], and then performed using two precursor salt solutions: solution 1 was contained 0.2 M of Ferric nitrate  $Fe(NO_3)_3 \cdot 9H_2O$  that prepared from dissolved 4.04 g in 50 mL D.W under ultrasonic waves for 10 min. Solution 2 was contained 0.1 M of Zinc nitrate  $Zn(NO_3)_2 \cdot 6H_2O$  that prepared from

Table 1. The General properties of alkali blue 4B dye.

Name	Alkali blue 4B dye
Hill Formula	C <sub>32</sub> H <sub>28</sub> N <sub>3</sub> NaO <sub>4</sub> S
Molar mass	573.64 g/mol
Dye class	Triarylmethane
Colour, λ <sub>max</sub> .	Dark blue, 593 nm
Structure	

dissolved 1.45 g in 50 mL D.W under ultrasonic waves for 10 min. Inside the ultrasonic bath, solution 2 was added step by step to solution 1 and mixed for 10 min. The pH of the produced solution was measured to be about 3, after

that, 0.5 g of Hexamethylene tetramine called also (methenamine or hexamine) as a non-ionic surfactant with a cage-like structure, was added as a capping agent and enhanced the growth of NP shape under continuous mixed using a magnetic

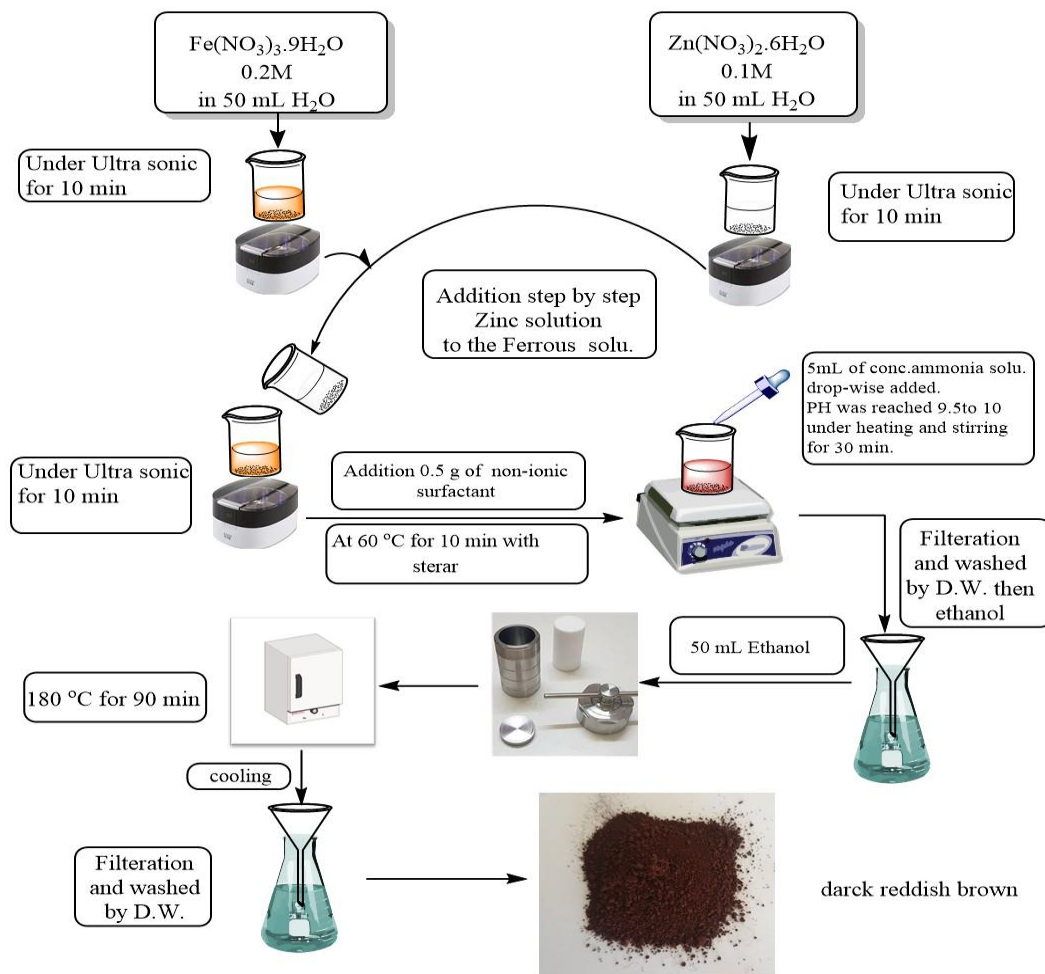
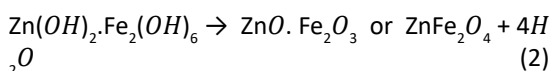
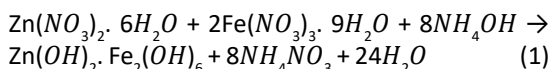


Fig. 1. The schematic diagram of the steps of zinc ferrite nanoparticle preparation.

stirrer at 60 °C for 10 min.

The pH of the solution must be fixed using conc. ammonia solution that drop-wise added, and reached to be about 9.5 to 10 under stirring continued for 30 min at 60 °C. The dark brown solution was produced; this solution was filtered and washed with D.W then ethanol. This precipitate was dispersive in 50 mL from Ethanol, then transported to a Teflon cup sealed in an autoclave of hydrothermal instrument and heated in the oven at 180 °C for 90 min. After cooling the steles steal autoclave in air, the solution was filtered and washed by 50 mL D.W to ensure all surfactant is removed, then 30 mL of ethanol to remove all humidity After that the dark reddish brown precipitate was thrown to dry using silica gel inside a desiccator overnight to get Zinc ferrite as powder. All of the steps for the preparation of zinc ferrite are shown in Fig. 1.

The chemical reactions of spinel ZnFe<sub>2</sub>O<sub>4</sub> formed were suggested using the following equations.



*Application of the Spinel ZnFe<sub>2</sub>O<sub>4</sub> used to decolorize alkali blue 4B dye solution*

A homemade photoreactor was used to carry out the photoreaction in Fig. 2. This photoreactor

is equipped with a 400-watt UV light ( light intensity equal to 1.87 x 10<sup>-7</sup> ensien.sec<sup>-1</sup>) that used a wooden box as a reactor’s body to prevent the UV-A light risk[13], with a magnetic stirrer, a Pyrex glass beaker (500 mL), a Teflon bar, and used two different fans to depress the heat and fixed the temperature of photoreactor [14-16].

The dark reaction is essential for the establishment to reach the reaction for the equilibrium adsorption condition[17-20]. This step was performed by magnetically agitating 25 ppm of alkali blue 4B dye with n g from spinel ZnFe<sub>2</sub>O<sub>4</sub> at pH 2.5 for 15 minutes. Following the adsorption stage, the suspension was exposed to UV light, and about 5 mL of aliquots were collected at 5 minute intervals until 30 minutes. The collected suspensions were centrifuged twice at 6000 rpm for 20 minutes. The absorbance of the resulting filters was measured at 593 nm using a UV-Vis spectrophotometer (FAITHFUL model 721). Equations 3 and 4 were used to get the apparent first order rate constant of this photoreaction and the efficiency of decolonization[21-26] respectively.

$$\ln \left( \frac{C_0}{C_t} \right) = k_{app}t \quad (3)$$

$$\text{PDE \%} = \frac{(C_0 - C_t)}{C_0} \times 100 \quad (4)$$

**RESULT AND DISCUSSION**

*Structure Properties*

According to Fig. 3, XRD analysis was used

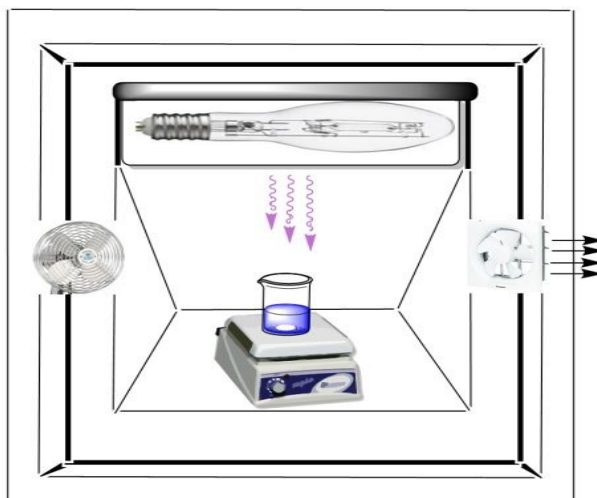


Fig. 2. Diagrammatic representation of a Homemade Photocatalytic Reactor Unit.

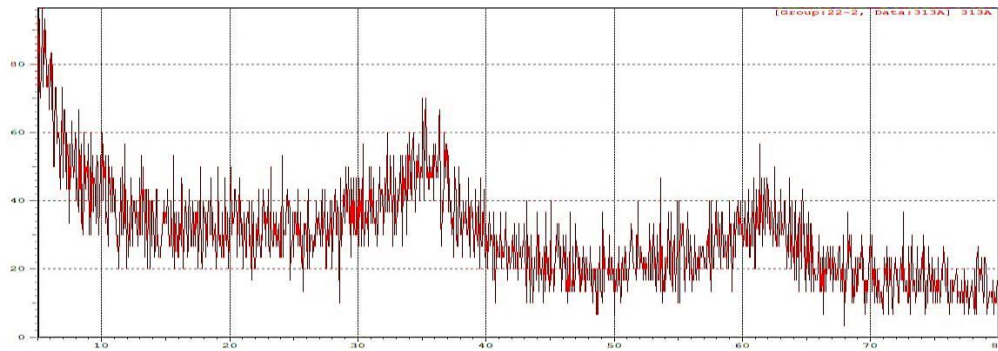


Fig. 3. XRD pattern of the normal spinel  $ZnFe_2O_4$  nanoparticle.

to determine the structure of prepared spinel  $ZnFe_2O_4$  ranging from  $0^\circ$  to  $80^\circ$  using a Lab X XRD 6000-Shimadzu. The analysis of XRD result was the  $ZnFe_2O_4$  peaks were embedded in an amorphous matrix that was due to no calcination. The results give low and broad peaks with diffraction patterns at  $2\theta$  of  $29.9^\circ$ ,  $35.30^\circ$ ,  $36.40^\circ$ ,  $42.78^\circ$ ,  $51.8^\circ$ ,  $55.05^\circ$  and  $62.2^\circ$  that ascribed to the reflection of (220), (311),  $(2\bar{2}\bar{2})$ , (400), (331), (422), and (440) planes of the spinel  $ZnFe_2O_4$ , respectively. These peaks are in agreement with results reported in references [27,28]. These results are in agreement with the FT-IR analysis that supported the prepared of normal spinel  $ZnFe_2O_4$ , which is discussed later. The mean crystallite size for spinel  $ZnFe_2O_4$  was calculated using the Scherer's equation(5) [29-33], and found to be equal 16.98 nm. This value proved the prepared spinel is nanomaterial and amorphous [34,35].

$$L = \frac{K \cdot \lambda}{\beta \cdot \cos\theta} \quad (5)$$

Where k, denotes the shape constant,  $\lambda$  is Cu's

wavelength used as a source of x-ray,  $2\theta$  is a Bragg diffraction angle, and (FWHM) is meaning a full width at half maximum intensity.

#### Morphology of studied photo catalyst surfaces SEM analysis

It was used to determine the morphology of the sample surface using (FESEM FEI Nova Nano SEM 450). The SEM images of spinel zinc ferrite surfaces display in Fig. 4. SEM reveals that the sample shows a compressed order of homogenous nanoparticles with an almost spherical agglomerated as a like-cauliflower nanoparticle shape. This growth of Zn ferrite nanoparticle depends on the properties of surfactant which leads to the form of this reasonable shape. Most particles are assembled, hence, the particle size is more than the mean crystal size [32, 34], and equal to 27.78 nm, this behaviour indicates the  $ZnFe_2O_4$  nanoparticles are polycrystalline in their structure.

#### EDX analysis

It was used to validate the sample's components.

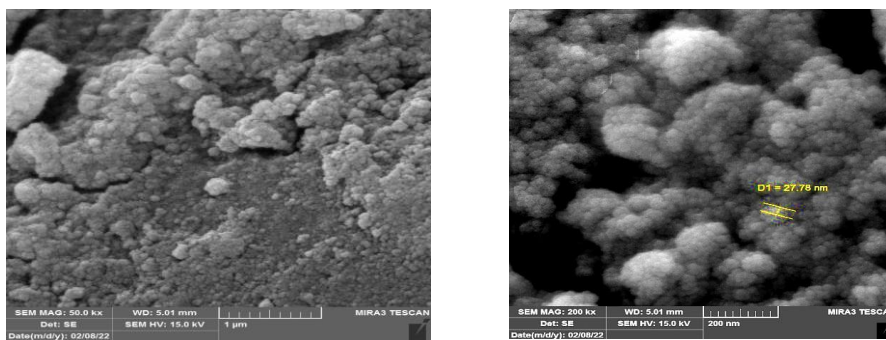


Fig. 4. SEM images the normal spinel  $ZnFe_2O_4$  nanoparticle.

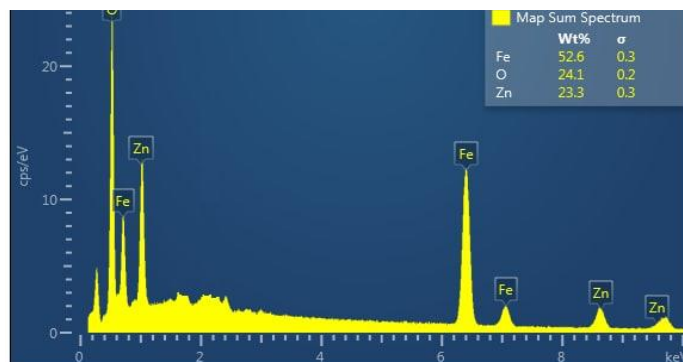


Fig. 5. The EDX spectrum of the normal spinel  $ZnFe_2O_4$  nanoparticle.

As seen in Fig. 5, the catalyst zinc ferrite consists Zn, Fe and O, without any impurities, this is good agreement those reported in references[36-38].

#### FT-IR spectrum of $ZnFe_2O_4$

Fig. 6 explains the FT-IR spectrum of  $ZnFe_2O_4$  powder. Two resemble bands  $590\text{ cm}^{-1}$  and  $655\text{ cm}^{-1}$  are observed as a characteristic of the normal spinel  $ZnFe_2O_4$ . The low-frequency band ( $590\text{ cm}^{-1}$ ) is an assignment to the stretching vibration of the chemical bond of ( $Fe^{3+} - O^{2-}$ ) in octahedral sites, while the higher frequency band ( $655\text{ cm}^{-1}$ ) is attributed to the stretching vibration of the chemical bond of ( $Zn^{2+} - O^{2-}$ ) in the tetrahedral sites. These results are in agreement with that previously reported, the range of wave numbers

for the interaction of metal-oxygen in crystal lattices are obtained for octahedral vibration mode and tetrahedral vibration mode at  $474\text{--}636\text{ cm}^{-1}$  and  $(550\text{--}750)\text{ cm}^{-1}$ , respectively [39,40]. Moreover, the peaks at  $3390\text{ cm}^{-1}$  and  $1620\text{ cm}^{-1}$  are beyond the stretching vibration and bending mode of water molecular[27]. The clear bands in the range of  $(1330 - 1346)\text{ cm}^{-1}$  and the band at  $1215\text{ cm}^{-1}$  can be associated with the C-H bending vibrations and C-N stretching vibration [41,42] in the used surfactant structure( Hexamine).

#### Optical Property of studied photocatalyst

##### The band gaps energy

The optical energy bandgaps (Eg in eV) were determined for all photocatalyst samples using

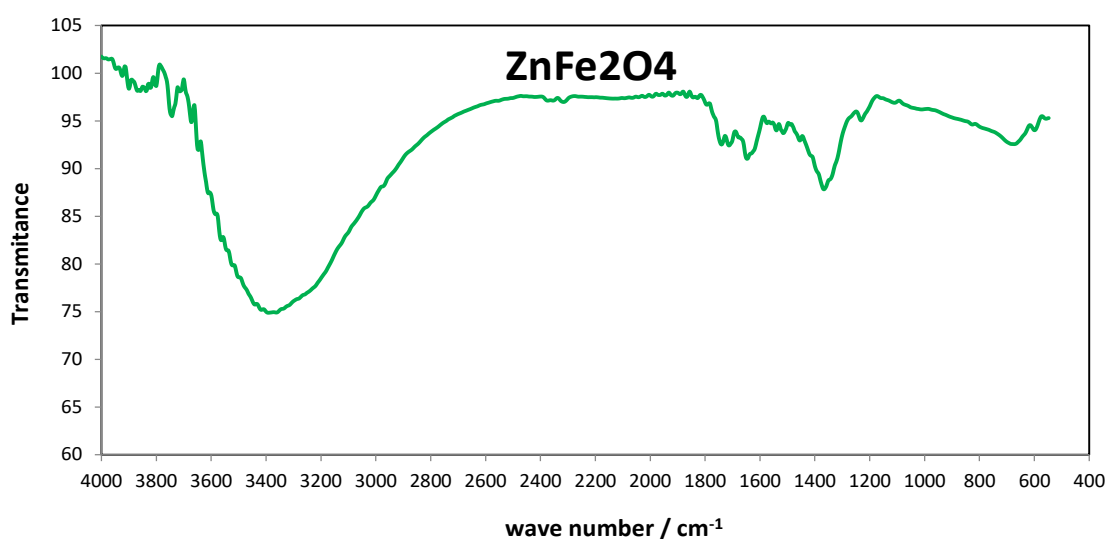


Fig. 6. FT-IR spectrum of prepared the normal spinel  $ZnFe_2O_4$  nanoparticle

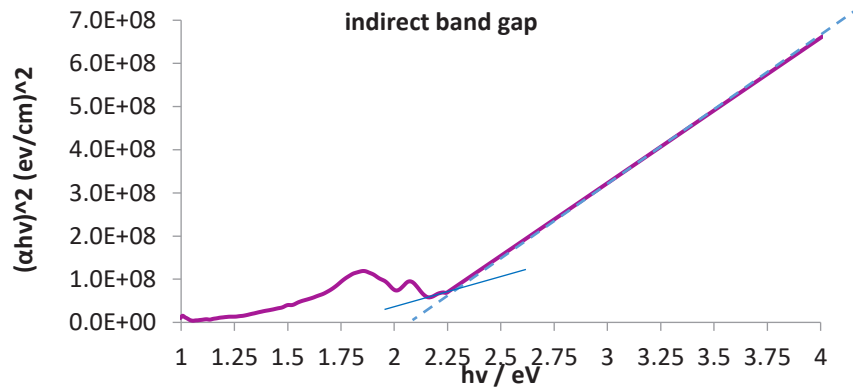


Fig. 7. Band gap of prepared the normal spinel  $ZnFe_2O_4$  nanoparticle.

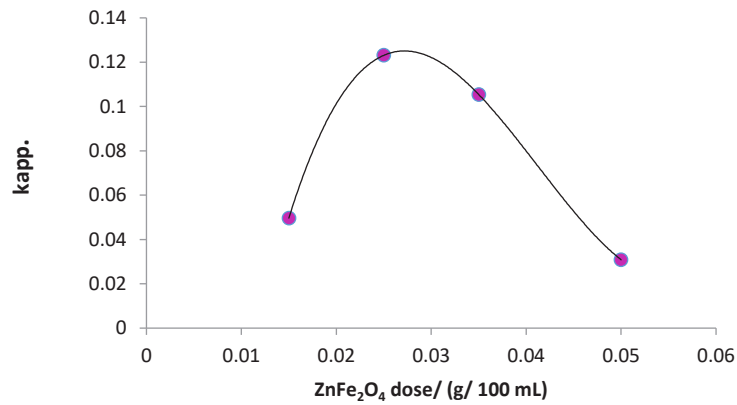


Fig.8. Effect of different dose of the normal spinel  $ZnFe_2O_4$  nanoparticle on photodecolorization rate constant ( $k_{app}$ ) of Alkali blue 4B dye.

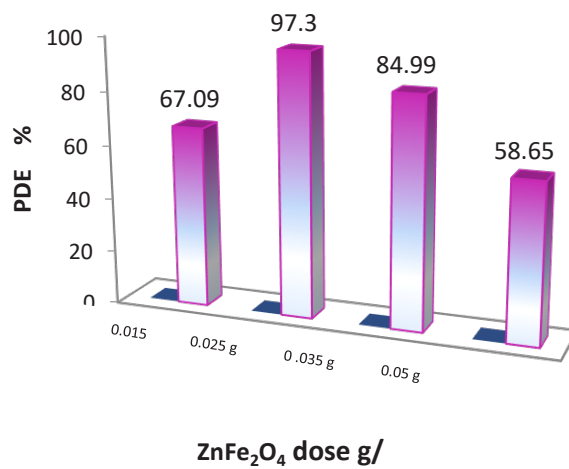


Fig.9. The relationship between (PDE %) and different dose of the normal spinel  $ZnFe_2O_4$  nanoparticle.

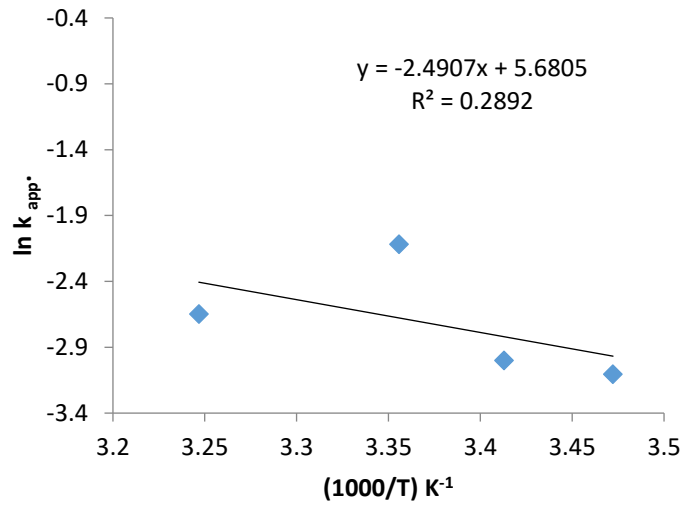


Fig.10. The Arrhenius equation plot for photoreaction in the presence of the normal spinel  $ZnFe_2O_4$  nanoparticle.

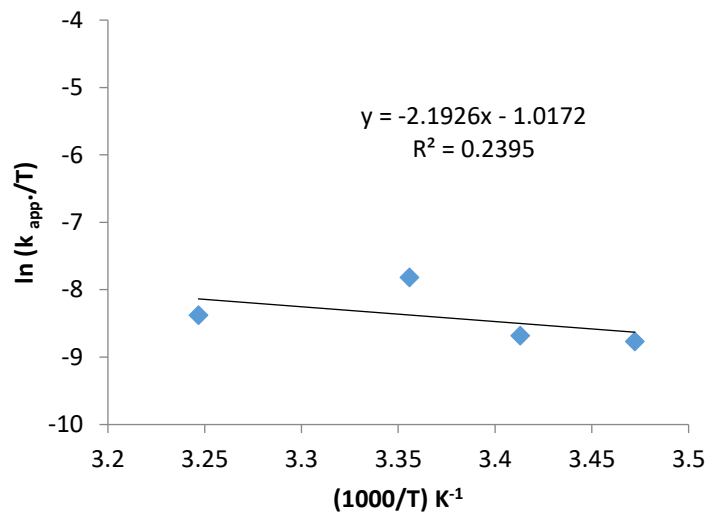


Fig.11. The Eyring-Polanyi equation plot for photoreaction in the presence of the normal spinel  $ZnFe_2O_4$  nanoparticle.

the Tauc equation[41-45], as seen in equations 6 and 7.

$$\alpha h\nu = k(h\nu - E_g)^m \quad (6)$$

$$\alpha = (2.3026 A)/t \quad (7)$$

Where ,  $h$  ,  $\nu$  ,  $k$  ,  $t$  ,  $A$  , and  $m$  are absorption

coefficient, Plank's constant the light, frequency, optical constant, thickness, the absorbance and constant value equal to  $\frac{1}{2}$  or 2 for direct and indirect transitions, respectively.

The equation 4 plotted in Fig. 7 and demonstrated that the band gap of prepared spinel  $ZnFe_2O_4$  nanoparticle is an indirect band gap[27] and equal to 2.15 eV, this value is in agreement



Table 2. The Calculated activation energy and thermodynamic functions for decolorization reaction of Alkali blue 4B dye with prepared the normal spinel ZnFe<sub>2</sub>O<sub>4</sub> nanoparticle.

Samples	E <sub>a</sub> /kJ mol <sup>-1</sup>	ΔH <sup>#</sup> /kJ mol <sup>-1</sup>	ΔS <sup>#</sup> /kJ mol <sup>-1</sup> K <sup>-1</sup>	ΔG <sup>#</sup> /kJ mol <sup>-1</sup>
ZnFe <sub>2</sub> O <sub>4</sub>	47.689	41.982	-0.205	103.369

with the value reported in reference [46].

#### Photo-decolorization of Alkali blue 4B dye

After determining the effectiveness of the prepared spinel ZnFe<sub>2</sub>O<sub>4</sub> Nanoparticle depended on measuring the optical properties like band gap, this spinel was applied in photo-decolorization of Alkali blue 4B dye. And that is by taking several weights from the photo catalyst and knowing the ideal weight for the removal, then applying the specified weight over a range of temperatures to find the thermodynamics functions. Several weights of the prepared spinel ZnFe<sub>2</sub>O<sub>4</sub> Nanoparticle (0.015, 0.025, 0.035, 0.05) g were taken. The rate of reaction and efficiency rises with increasing the dose, as shown in Figs. 8 and 9. That attitude raises the active site surface, which leads to increase the interaction between the dye and hydroxyl radicals on the photocatalyst surface [45]. The appropriate weight occurred 0.025g with the efficiency equal to 97.3. On the other hand, the increment in spinel ZnFe<sub>2</sub>O<sub>4</sub> Nanoparticle dose of more 0.025 g causes declining in efficiency, that due to increase the in the turbidity of the solution, which depresses of penetration of light through the solution this effect is called the screen effect [25, 47,48].

After choosing the ideal weight of the photocatalyst and applying the reaction over a range of temperatures (15, 20, 25, 35) °C, it was found that the best temperature for the reaction is 25 °C. Based on figs. 10 and 11, the Arrhenius equation plot [48-51], and Eyring-Polanyi equation plot [52,53] were done to calculate activation energy and thermodynamic functions listed in Table 2. From the results, it was found that the photoreaction is endothermic, non-spontaneous, and less random and has low activation energy. The positive values of ΔH<sup>#</sup> and ΔG<sup>#</sup> are in agreement with data published in references [47,53,54], this conduct is beyond incrementing the solvation of transition state between dye molecules and hydroxyl radical species [45,55,56].

#### CONCLUSION

The main conclusions from this manuscript can

be summarized by:

- 1- Preparation of normal spinel ZnFe<sub>2</sub>O<sub>4</sub> as nanoparticles like cauliflower using precipitation method-assisted hydrothermal method in the presence of ethanol and capping agent (hexamine) as non-polar surfactant.
- 2- The normal spinel ZnFe<sub>2</sub>O<sub>4</sub> nanoparticle is proved using XRD analysis and SEM-EDX.
- 3- The FT-IR analysis has supported the synthesis of normal spinel ZnFe<sub>2</sub>O<sub>4</sub> nanoparticle depending on octahedral and tetrahedral sites for Metal interaction Oxygen in lattices.
- 4- The normal spinel ZnFe<sub>2</sub>O<sub>4</sub> nanoparticle can be used as a photocatalyst depending on the calculated band gap, which has been an indirect type.
- 5- The photoactivity of normal spinel ZnFe<sub>2</sub>O<sub>4</sub> nanoparticle increases with increased dose then decreases.
- 6- The photoreaction is obeyed pseudo-first order kinetic with low activation energy and endothermic reaction.

#### ACKNOWLEDGMENTS

The Authors gratefully acknowledge all personnel who support this manuscript in the University of Kerbala's faculty of science-department of chemistry and department of physics.

#### CONFLICT OF INTEREST

The authors declare that there is no conflict of interests regarding the publication of this manuscript.

#### REFERENCES

1. Fadlalla MI, Senthil Kumar P, Selvam V, Ganesh Babu S. Recent Advances in Nanomaterials for Wastewater Treatment. Environmental Chemistry for a Sustainable World: Springer International Publishing; 2019. p. 21-58.
2. Jeseentharani V, George M, Jeyaraj B, Dayalan A, Nagaraja KS. Synthesis of metal ferrite (MFe<sub>2</sub>O<sub>4</sub>, M = Co, Cu, Mg, Ni, Zn) nanoparticles as humidity sensor materials. J Exp Nanosci. 2013;8(3):358-370.
3. Zhang G, Li C, Cheng F, Chen J. ZnFe<sub>2</sub>O<sub>4</sub> tubes: Synthesis and application to gas sensors with high sensitivity and low-energy consumption. Sensors Actuators B: Chem. 2007;120(2):403-410.

4. Yelenich OV, Solopan SO, Kolodiaznyy TV, Dzyublyuk VV, Tovstolytkin AI, Belous AG. Magnetic properties and high heating efficiency of ZnFe<sub>2</sub>O<sub>4</sub> nanoparticles. *Materials Chemistry and Physics*. 2014;146(1-2):129-135.
5. Shawabkeh RA. Adsorption of chromium ions from aqueous solution using activated carbo-aluminosilicate material. *NATO Security through Science Series: Springer Netherlands*. p. 249-254.
6. Guskos N, Glenis S, Typek J, Zolnierkiewicz G, Berczynski P, Wardal K, et al. Magnetic properties of ZnFe<sub>2</sub>O<sub>4</sub> nanoparticles. *Open Physics*. 2012;10(2).
7. Haghniaz R, Rabbani A, Vajhadin F, Khan T, Kousar R, Khan AR, et al. Anti-bacterial and wound healing-promoting effects of zinc ferrite nanoparticles. *Journal of Nanobiotechnology*. 2021;19(1).
8. Din MI, Jabbar S, Najeeb J, Khalid R, Ghaffar T, Arshad M, et al. Green synthesis of zinc ferrite nanoparticles for photocatalysis of methylene blue. *International Journal of Phytoremediation*. 2020;22(13):1440-1447.
9. Deng W, Xiong K, Ge N, Yu M, Chen L, Wang J. Cobalt and titanium co-doped zinc ferrite film photoanode with boosted interfacial photoelectrocatalytic activity for efficient degradation of tetracycline via the covalency competition in the Zn-O-Fe backbone. *Chem Eng J*. 2022;433:134456.
10. Anchieta C, Cancelier A, Mazutti M, Jahn S, Kuhn R, Gündel A, et al. Effects of Solvent Diols on the Synthesis of ZnFe<sub>2</sub>O<sub>4</sub> Particles and Their Use as Heterogeneous Photo-Fenton Catalysts. *Materials*. 2014;7(9):6281-6290.
11. Tatarchuk T, Bououdina M, Judith Vijaya J, John Kennedy L. Spinel Ferrite Nanoparticles: Synthesis, Crystal Structure, Properties, and Perspective Applications. *Springer Proceedings in Physics: Springer International Publishing*; 2017. p. 305-325.
12. Sinthiya MM RK, Mathuri S, Manimozhi T, Kumaresan N, Margoni MM, Karthika PC. Synthesis of zinc ferrite (ZnFe<sub>2</sub>O<sub>4</sub>) nanoparticles with different capping agents. *International Journal of ChemTech Research* 7(5):2144-2149.
13. Hussain ZA, Fakhri FH, Alesary HF, Ahmed LM. ZnO Based Material as Photocatalyst for Treating the Textile Anthraquinone Derivative Dye (Dispersive Blue 26 Dye): Removal and Photocatalytic Treatment. *Journal of Physics: Conference Series*. 2020;1664(1):012064.
14. Jawad TM, R. Al-Lami M, Hasan A, Al-Hilifi J, Mohammad R, Ahmed L. Synergistic Effect of dark and photoreactions on the removal and photo-decolorization of azo carmosine dye (E122) as food dye using Rutile- TiO<sub>2</sub> suspension. *Egyptian Journal of Chemistry*. 2021;0(0):0-0.
15. Alattar R, Saleh H, Al-Hilifi J, Ahmed L. Influence the addition of Fe<sup>2+</sup> and H<sub>2</sub>O<sub>2</sub> on removal and decolorization of textile dye (dispersive yellow 42 dye). *Egyptian Journal of Chemistry*. 2020;0(0):0-0.
16. Jaafar MT, Ahmed LM. Reduced the toxicity of acid black (nigrosine) dye by removal and photocatalytic activity of TiO<sub>2</sub> and studying the effect of pH, temperature, and the oxidant agents. *INTERNATIONAL CONFERENCE OF NUMERICAL ANALYSIS AND APPLIED MATHEMATICS ICNAAM 2019: AIP Publishing*; 2020.
17. Ahmed L, Kadhim H, Al-Hachamii M. Facile Synthesis of Spinel CoCr<sub>2</sub>O<sub>4</sub> and Its Nanocomposite with ZrO<sub>2</sub>: Employing in Photo-catalytic Decolorization of Fe (II)-(luminol-Tyrosine) Complex. *Egyptian Journal of Chemistry*. 2021;65(1):481-488.
18. Alattar RA, Hassan ZM, Abass SK, Ahmad LM. Synthesis, characterization and study the photodecolorization of Schiff base Fe(III) complex in ZnO/UV-A light system. *International conference of numerical analysis and applied mathematics icnaam 2019: AIP Publishing*; 2020.
19. Ahmed LM, Saeed SI, Marhoon AA. Effect of Oxidation Agents on Photo-Decolorization of Vitamin B12 in the Presence of ZnO/UV-A System. *Indonesian Journal of Chemistry*. 2018;18(2):272.
20. Ahmed L, S. Fadhil E, F. Mohammed A. Effect of silver doping on structural and photocatalytic circumstances of ZnO nanoparticles. *Iraqi Journal of Nanotechnology*. 2020(1):13-20.
21. Karam F, Saeed N, Al Yasasri A, Ahmed L, Saleh H. Kinetic Study for Reduced the Toxicity of Textile Dyes (Reactive yellow 14 dye and Reactive green dye) Using UV-A light/ZnO System. *Egyptian Journal of Chemistry*. 2020;0(0):0-0.
22. Marhoon AA, Saeed, S. I., and Ahmed, L. M. Application of some effects on the Degradation of the aqueous solution of Fuchsine dye by photolysis. *Journal of Global Pharma Technology*. 2011;11(9):76-81.
23. Hussein ZA, Abbas SK, Ahmed LM. UV-A activated ZrO<sub>2</sub> via photodecolorization of methyl green dye. *IOP Conference Series: Materials Science and Engineering*. 2018;454:012132.
24. Jasim KM, Ahmed LM. TiO<sub>2</sub> Nanoparticles Sensitized by Safranin O Dye using UV-A Light System. *IOP Conference Series: Materials Science and Engineering*. 2019;571(1):012064.
25. Abass SK, Al-Hilifi JA, Abbas SK, Ahmed LM. Preparation, Characterization and Study of the Photodecolorization of Mixed-Ligand Binuclear Co(II) Complex of Schiff Base by ZnO. *Indonesian Journal of Chemistry*. 2020;20(2):404.
26. Sawsan Khudhair Abbas ZMH, Luma M Ahmed. Influencing the Artificial UV-A light on decolorization of Chlorazol black BH Dye via using bulk ZnO Suspensions. *Journal of Physics: Conference Series*. 2019;1294(5):052050.
27. Rachna, Singh NB, Agarwal A. Preparation, Characterization, Properties and Applications of nano Zinc Ferrite. *Materials Today: Proceedings*. 2018;5(3):9148-9155.
28. C. Sambathkumar SEA, B. Natarajan, A. Arivarasan, P. Devendran. Examination Of Structural Morphological and Magnetic Behaviour of ZnFe<sub>2</sub>O<sub>4</sub> Nanoparticle Synthesised by Co-Precipitation Method. *International Journal of Engineering and Advanced Technology*. 2019;9(154):1085-1088.
29. Ahmed L, Hussein F, Mahdi A. Photocatalytic Dehydrogenation of Aqueous Methanol Solution by Naked and Platinized TiO<sub>2</sub> Nanoparticles. *Asian J Chem*. 2012;24(12):5564.
30. Jassim S, Abbas A, Al-Shakban M, Ahmed L. Chemical Vapour Deposition of CdS Thin Films at Low Temperatures from Cadmium Ethyl Xanthate. *Egyptian Journal of Chemistry*. 2021;64(5):3-4.
31. Ahmed LM, Ivanova I, Hussein FH, Bahnemann DW. Role of Platinum Deposited on TiO<sub>2</sub> in Photocatalytic Methanol Oxidation and Dehydrogenation Reactions. *International Journal of Photoenergy*. 2014;2014:1-9.
32. Ahmed L, Ali S, Ali M. Hybrid Phosphotungstic acid -Dopamine (PTA-DA) Like-flower Nanostructure Synthesis as a Furosemide Drug Delivery System and Kinetic Study of Drug Releasing. *Egyptian Journal of Chemistry*. 2021;64(10):5547-5553.

33. Ahmed L, Alkhafaji E, Oda N. Characterization of silver nanohybrid with layers double hydroxide and demonstration inhibition of antibiotic-resistance Staphylococcus aureus. *Egyptian Journal of Chemistry*. 2022;65(6):1-2.
34. Obaid A, Ahmed L. One-Step Hydrothermal Synthesis of  $\alpha$ - $\text{MoO}_3$  Nano-belts with Ultrasonic Assist for incorporating  $\text{TiO}_2$  as a NanoComposite. *Egyptian Journal of Chemistry*. 2021;64(10):5725-5734.
35. Mohammad H, Saeed S, Ahmed L. Broccoli-like Iron Oxide Nanoparticles Synthesis in Presence of Surfactants and Using Them in the Removal of Water-Colored Contamination. *Journal of Nanostructures*. 2022;12(4):1034-1048.
36. Kumar GSY, Naik HSB, Roy AS, Harish KN, Viswanath R. Synthesis, Optical and Electrical Properties of  $\text{ZnFe}_2\text{O}_4$  Nanocomposites. *Nanomaterials and Nanotechnology*. 2012;2:19.
37. Manikandan A, Judith Vijaya J, Sundararajan M, Meganathan C, Kennedy LJ, Bououdina M. Optical and magnetic properties of Mg-doped  $\text{ZnFe}_2\text{O}_4$  nanoparticles prepared by rapid microwave combustion method. *Superlattices Microstruct*. 2013;64:118-131.
38. Pascuta P, Vladescu A, Borodi G, Culea E, Tetean R. Structural and magnetic properties of zinc ferrite incorporated in amorphous matrix. *Ceram Int*. 2011;37(8):3343-3349.
39. Husain S, Yusup M, Haryanti NH, Suryajaya, Saukani M, Rodiansono, et al. Characteristics of zinc ferrite nanoparticles ( $\text{ZnFe}_2\text{O}_4$ ) from natural iron ore. *IOP Conference Series: Earth and Environmental Science*. 2021;758(1):012001.
40. Goodarz Naseri M, Saion EB, Kamali A. An Overview on Nanocrystalline  $\text{ZnFe}_2\text{O}_4$ ,  $\text{MnFe}_2\text{O}_4$ , and  $\text{CoFe}_2\text{O}_4$  Synthesized by a Thermal Treatment Method. *ISRN Nanotechnology*. 2012;2012:1-11.
41. Ezzayani K, Ben Khelifa A, Saint-Aman E, Loiseau F, Nasri H. Complex of hexamethylenetetramine with magnesium-tetraphenylporphyrin: Synthesis, structure, spectroscopic characterizations and electrochemical properties. *J Mol Struct*. 2017;1137:412-418.
42. Jawad TM, Ahmed LM. Direct ultrasonic synthesis of  $\text{WO}_3/\text{TiO}_2$  nanocomposites and applying them in the photodecolorization of eosin yellow dye. *Periódico Tchê Química*. 2020;17(34):621-633.
43. Hayawi MK, Kareem MM, Ahmed LM. Synthesis of spinel  $\text{Mn}_3\text{O}_4$  and spinel  $\text{Mn}_3\text{O}_4/\text{ZrO}_2$  nanocomposites and using them in photo-catalytic decolorization of Fe(II)-(4,5-diazafluoren-9-one 11) complex. *Periódico Tchê Química*. 2020;17(34):689-699.
44. Kadhim H, Ahmed L, Al-Hachamii M. Facile Synthesis of Spinel  $\text{CoCr}_2\text{O}_4$  and Its Nanocomposite with  $\text{ZrO}_2$ : Employing in Photo-catalytic Decolorization of Fe (II)-(luminol-Tyrosine) Complex. *Egyptian Journal of Chemistry*. 2022;65(1):481-488.
45. Fakhri FH, Ahmed LM. Incorporation  $\text{CdS}$  with  $\text{ZnS}$  as Composite and Using in Photo-Decolorization of Congo Red Dye. *Indonesian Journal of Chemistry*. 2019;19(4):936.
46. Ridha NJ, Mohamad Alosfur FK, Kadhim HBA, Ahmed LM. Synthesis of Ag decorated  $\text{TiO}_2$  nanoneedles for photocatalytic degradation of methylene blue dye. *Materials Research Express*. 2021;8(12):125013.
47. Daruka Prasad B, Nagabhushana H, Thyagarajan K, Nagabhushana BM, Jnaneshwara DM, Sharma SC, et al. Magnetic and dielectric interactions in nano zinc ferrite powder: Prepared by self-sustainable propellant chemistry technique. *J Magn Magn Mater*. 2014;358-359:132-141.
48. Ahmed LM. Photo-Decolorization Kinetics of Acid Red 87 Dye in  $\text{ZnO}$  Suspension Under Different Types of UV-A Light. *Asian J Chem*. 2018;30(9):2134-2140.
49. Sharma SK, Bhunia H, Bajpai PK.  $\text{TiO}_2$ -assisted Photocatalytic Degradation of Diazo Dye Reactive Red 120: Decolorization Kinetics and Mineralization Investigations. *Journal of Advanced Oxidation Technologies*. 2013;16(2).
50. Bensouyad H, Bensaha R. Enhanced Structural, Optical, And Photocatalytic Activities Of  $\text{CuO}/\text{TiO}_2:\text{ZrO}_2$  Catalysts For Degrading Methyl Orange (MO) Dye Under UV-Visible Irradiation. *Research Square Platform LLC*; 2022.
51. Saeed SI, Attol DH, Eesa MT, Ahmed LM. Zinc oxide-mediated removal and photocatalytic treatment of direct orange 39 dye as a textile dye. *International conference of computational methods in sciences and engineering iccmse 2021*: AIP Publishing; 2023.
52. Ahmed DS, Mohammed MR, Mohammed MKA. Synthesis of Multi-walled Carbon Nanotubes Decorated with  $\text{ZnO}/\text{Ag}$  Nanoparticles by Co-precipitation Method. *Nanoscience & Nanotechnology-Asia*. 2020;10(2):127-133.
53. Al-Senani GM, Al-Fawzan FF, Almufarj RS, Abd-Elkader OH, Deraz NM. Biosynthesis, Physicochemical and Magnetic Properties of Inverse Spinel Nickel Ferrite System. *Crystals*. 2022;12(11):1542.
54. Kzar KO, Mohammed ZF, Saeed SI, Ahmed LM, Kareem DI, Hadyi H, et al. Heterogeneous photo-decolorization of cobaltous phthalocyaninate dye (reactive green dye) catalyzed by  $\text{ZnO}$ . The 7th international conference on applied science and technology (ICAST 2019): AIP Publishing; 2019.
55. Bousalah D, Yeddou AR, Hachemi M, Chergui A, Nadjemi B. Oxidation of azo dye carmoisine (e122) in aqueous solution by heterogeneous catalyst  $\text{CuO}/\text{Al}_2\text{O}_3$  system. *Environmental Engineering and Management Journal*. 2021;20(2):167-175.
56. Obaid AJ, Ahmed LM.  $\text{TiO}_2$  - Catalyzed photo decolorization of chlorazol black BH dye under UV-A light. The 9th international conference on applied science and technology (ICAST 2021): AIP Publishing; 2022.